International Journal for Housing Science and Its Applications
Publish August 6, 2025. Volume 46, Issue 3 Pages 5044-5054

https://doi.org/10.70517/ijhsa463432

Multi-objective optimization design of soft magnetic composite reactors based on intelligent algorithms

Yangyang Ma[1], Wenle Song[1], Jie Gao[2,*], Yang Liu[2], Yilei Shang[2], Weimei Zhao[2] and Fuyao Yang[2]
[1] State Grid Cangzhou Electric Power Supply Company, Cangzhou, Hebei, 061000, China
[2] China Electric Power Research Institute, Beijing, 100192, China

Corresponding authors: (e-mail: conch3501@163.com).

Abstract This paper proposes a comprehensive electromagnetic-noise optimization design method based on the forgotten least squares method for the electromagnetic performance and vibration-noise synergistic optimization problems faced by Fe-based soft magnetic composite core reactors in high frequency applications. The nonlinear magnetization model of the core material is constructed through experiments, and the magnetic-mechanical coupling kinetic equations are established by combining Maxwell's system of equations and mechanical vibration theory. The least squares method incorporating the forgetting factor is used to identify the parameters of the two-inertia mechanical system, and adaptive filtering is realized with the help of parameter sensitivity analysis. Simulation experimental results show that the sound insulation using the scheme of this paper can be up to 14.6dB(A), and the total sound pressure level of measurement points B and C at 1m outside the reactor cabinet after optimization is reduced by 10.2dB(A) and 11.5dB(A) respectively compared with the pre-optimization period, and its comprehensive noise reduction effect reaches more than 10.9dB(A), while the temperature rise is controlled within a reasonable range, which verifies the validity of the methodology and the applicability of engineering.

Index Terms Fe-based soft magnetic composites, core reactor, forgetting factor, least squares method, electromagnetic noise optimization

I. Introduction

With the development and upgrading of urban power distribution systems, reactors are widely used [1]. At the same time, the electromagnetic and vibration noise problems caused by reactors have attracted more and more attention, which not only become a safety issue, but also cause pollution to the surrounding environment. Therefore, the electromagnetic and noise optimization design becomes more important, and the application of Fe-based soft magnetic composites makes this optimization possible [2]-[5].

The traditional method of reactor design is only limited to designing the function and modeling of the product, and does not consider its dynamic characteristics. After the product is designed, it is then subjected to noise reduction, which requires changing the local or overall design of the product, increasing the cost, extending the product development cycle, and decreasing the competitiveness of the product [6]-[9]. For this reason, it is necessary to predict the dynamic characteristics at the product design stage, so as to realize the optimal design of the product and improve the economic efficiency [10], [11]. Fe-based soft magnetic composites, a kind of composite material composed of a soft magnetic matrix and a non-magnetic cladding layer [12]. The soft magnetic matrix is usually made of ferrite materials or amorphous alloys, while the nonmagnetic cladding layer can be made of materials such as oxides, nitrides, or polymers [13], [14]. This composite structure can effectively suppress the eddy current loss and increase the permeability and saturation magnetic induction strength of the material, which results in soft magnetic composites with excellent magnetic properties, low hysteresis, low eddy current loss, and high saturation magnetic induction strength, and thus has attracted much attention and focus, and has been widely used in the integrated optimal design of electromagnetic and noise in reactors [15]-[18]. However, so far, the optimal design of electromagnetic and vibration noise is still one of the world problems of core reactors, and although there are some mature theories and technological improvement measures, there are few researches on the complete realization of its vibration noise description from the perspective of numerical simulation so as to achieve the purpose of vibration and noise reduction [19]-[22].

In this paper, the nonlinear magnetization model of Fe-based soft magnetic composites is firstly constructed through magnetic property measurement experiments. Combining Maxwell's system of equations and mechanical vibration theory, the dynamic equations of the magneto-mechanical coupled system are established to reveal the vibration noise characteristics of the reactor. The parameters of the two-inertia mechanical system are identified

online by the forgotten least squares method, and the dynamic forgetting factor characteristic is utilized to suppress the saturation effect of historical data. The key design variables are identified through parameter sensitivity analysis to achieve electromagnetic-noise co-optimization.

II. Electromagnetic and noise optimization design of core reactor based on the least squares method

With the development of power electronics technology in the direction of high-frequency and large-capacity, the electromagnetic performance and operational stability of the reactor, as a core component of the power conversion and transmission system, have attracted much attention.Fe-based soft magnetic composites are widely used in reactor core design due to their excellent characteristics, such as high permeability and low loss. However, the magnetostrictive effect and electromagnetic force generated by the core under the action of alternating magnetic field lead to serious vibration and noise problems, which not only affects the reliability and service life of the equipment, but also may cause acoustic pollution to the surrounding environment. Therefore, how to realize the synergistic optimization of electromagnetic performance and noise characteristics has become a key issue to be solved in the design of Fe-based soft magnetic composite reactors.

Electromagnetic design focuses on the improvement of core loss and saturation characteristics, while noise control relies on structural damping or magnetic circuit adjustment. However, the multi-physics field coupling mechanism between electromagnetic field and mechanical vibration is complex, and it is difficult to realize the decoupling optimization of the two by traditional methods. In addition, the nonlinear magnetic properties of the core material and the time-varying nature of the dynamic mechanical response further increase the difficulty of parameter identification and model accuracy control. In recent years, data-driven optimization methods have gradually emerged, and this paper proposes a comprehensive electromagnetic-noise optimization scheme based on the forgotten least squares method, aiming to break through the technical bottleneck of multi-physics field coupling modeling and dynamic parameter identification.

II. A.Modeling of magneto-mechanical coupled system of core reactor

II. A. 1) Measurement of magnetic properties of core material samples

The magnetization characteristic represents the non-linear relationship between the magnetic field strength H and the magnetic induction strength B of a ferromagnetic material, also known as the $B-H$ curve, which can be measured experimentally. The magnetization curve of the sample is measured by the test system by placing the sample into the cavity of the test system and providing an external excitation for the excitation coil, which generates a changing magnetic field in the coil. In this paper, the magnetic properties of a test specimen of Fe-based soft magnetic composites (the material used to make the reactor core in this paper) are measured by using a magnetic property measurement device under the excitation of 50 Hz industrial frequency AC current.

The test system consists of three parts: the main unit, the measuring device, and the laser transmitter-receiver. The yoke of the measurement device consists of material samples stacked on top of each other, and the test specimen is in contact with the yoke through a cavity formed by a coil, which is held in place by a clamp at one end and is free to expand and contract at the other end. The coil contains an excitation winding and an induction winding, the magnetic field generated by the excitation winding along the length of the sample through the sample and the yoke iron to form a closed loop, by changing the size of the voltage of the excitation winding to control the size of the magnetic field strength and make the sample magnetic field gradually saturated; the induction coil by detecting the changes in the induction voltage and then get the sample of the magnetic induction strength and magnetic field strength.

In the externally applied magnetic field less than 500A / m when the magnetic induction strength of the material samples and the magnetic field strength is proportional to the relationship, but when the applied magnetic field is greater than 500A / m when the magnetic induction strength of the material samples is no longer with the magnetic field strength of the linear increase in the saturation state, but tends to saturation, so the material samples in the saturation of the unit area of the energy storage capacity decreases.

The magnetization characteristic curve of the material sample is fitted as a function of the magnetic field strength and substituted into the finite element analysis calculation, which makes the test data as close as possible to the characteristics of the core when it is actually working and ensures the accuracy of the simulation results.

II. A. 2) Electromagnetic analysis

The engineering electromagnetic field is a macroscopic sense of the electromagnetic field that can represent a practical problem, generally represented by Maxwell's system of equations, with two forms of expression: differential and integral. The integral form of Maxwell's equations is a set of characteristic equations describing the overall correspondence between the electromagnetic field and the field source from a macroscopic point of view, while the

differential form is a set of characteristic equations describing the field between the field quantity and the field source at each point in the field from a microscopic point of view. The differential form of the system of equations is an important method for solving local characteristic problems, and the finite element method is based on the mathematical model of Maxwell's differential form. Maxwell's system of equations consists of Ampere's loop law, Faraday's law of electromagnetic induction, the principle of continuity of magnetic flux, and Gauss's law, whose differential form of Maxwell's equations is for each point in the field. The differential form of Maxwell's system of equations is:

$$\begin{cases} \nabla \times H = J + \dfrac{\partial D}{\partial t} \\ \nabla \times E = -\dfrac{\partial B}{\partial t} \\ \nabla \cdot B = 0 \\ \nabla \cdot D = \rho \end{cases} \tag{1}$$

where H denotes the magnetic field strength (A/m); D denotes the potential shift vector (C/m²); J denotes the current density (A/m²); E denotes the electric field strength (V/m); and B denotes the magnetic induction strength (T); and ρ denotes the charge density (C/m²).

The set of Maxwell's equations reveals the fundamental laws of the electromagnetic field in space, and the equations are not independent of each other, but are interrelated and interact with each other. In a certain medium, the equations for the relationship between the potential shift vector and the electric field strength, the relationship between the magnetic induction strength and the magnetic field strength, and the relationship between the current density and the electric field strength are shown in equation (2).

$$\begin{cases} D = \varepsilon E = \varepsilon_r \varepsilon_0 E \\ B = \mu H = \mu_r \mu_0 H \\ J = \gamma E \end{cases} \tag{2}$$

where ε denotes the dielectric constant of the medium (F/m), $\varepsilon = \varepsilon_r \varepsilon_0$, ε_r denotes the relative dielectric constant, and ε_0 denotes the dielectric constant of the vacuum, which is generally used in the In the calculation process, $\varepsilon_0 \approx 8.854 \times 10^{-12} (F/m)$; μ denotes the magnetic permeability (H/m) of the conducting medium, $\mu = \mu_r \mu_0$, and μ_r denotes the relative magnetic permeability, μ_0 denotes the vacuum magnetic permeability, generally in the calculation process, $\mu_0 = 4\pi \times 10^{-7} (H/m)$; and γ denotes the electrical conductivity of the conducting medium (S/m).

Since the core reactor studied in this paper is excited by an alternating current of 50 Hz at the industrial frequency and the harmonic components do not reach the high frequency range, that is, the electromagnetic field changes slowly with time, the displacement current is negligible compared with the conduction current. So the electromagnetic field studied in this paper can be considered as a steady state field, i.e. $\partial D / \partial t = 0$. Therefore the first equation in Eq. (1) can be written as:

$$\nabla \times H = J \tag{3}$$

From the third equation in Eq. (1), $\nabla \cdot B = 0$, it is clear that the scatter of the magnetic induction intensity is zero, i.e., the flux of the magnetic field is zero, and the source of flux that produces the magnetic field does not exist. From the vector constancy equation, it follows that the scatter of the spin of any vector function is constantly equal to zero. In order to be able to calculate the magnetic field in space quantitatively, therefore, the vector magnetic potential $A(Wb/m)$ is introduced, then the magnetic induction strength B can be expressed by the spin of the vector magnetic potential function A, i.e.:

$$B = \nabla \times A \tag{4}$$

Substituting Eq. (4) into Eq. (1) and from the relationship $B = \mu H$ between the magnetic induction intensity vector and the magnetic field intensity vector, the Poisson's equation for the static magnetic field is given as:

$$\nabla \times \nu \nabla \times A = J \tag{5}$$

where $\nu = 1/\mu$ is the magnetoresistivity of the medium.

The magnetoresistivity of a nonlinear ferromagnetic material is not only a function of spatial coordinates, but also a function of the magnetic induction intensity.

The corresponding boundary conditions for the electromagnetic field are:

$$\begin{cases} \Omega : \nabla \times \nu \nabla \times A = J \\ \Gamma_1 : A = A_o \\ \Gamma_2 : H \times n = q \\ \Gamma_3 : H \times n = f_0(A) \end{cases} \tag{6}$$

where A_o, q and $f_0(A)$ are the known distribution functions on the boundaries Γ_1, Γ_2, and Γ_3, respectively, and n is the outer normal of the boundary direction.

Solving Poisson's equation with the given magnetic field boundary conditions yields the vector magnetic potential and other electromagnetic variables at any point.

II. B.Reactor vibration noise characteristics

II. B. 1) Effect of magnetostriction on core vibration noise

Magnetostrictive materials are ferromagnetic materials whose dimensions change significantly in the direction of the magnetic field as the alternating magnetic field changes periodically. In this paper, the magnetostriction of the test samples in the Fe-based soft magnetic composite core reactor is proportional to the square of the loading voltage, and the frequency is two times of the voltage frequency.

II. B. 2) Effect of Maxwell's force on reactor vibration noise

The reactor has an air gap and is anisotropic poles at all times, and the Maxwell forces on the upper and lower surfaces of neighboring core cakes are attractive forces of magnitude:

$$F_M = \frac{B^2 S}{2\mu_0} = \frac{\phi^2}{2\mu_0 S} \tag{7}$$

where, F_M is the magnitude of Maxwell's force; μ_0 is the vacuum permeability with magnitude $4\times10^{-7}\ H/m$; B is the magnetic flux density; S is the magnetic flux area; and ϕ is the magnetic flux.

At the time when the reactor is subjected to an AC voltage with an angular frequency of $\omega = 2\pi f$, $\phi = \phi_m \sin \omega t$, and ϕ_m is the peak magnetic flux.

Substituting into Eq. (7) yields:

$$F_M = \frac{\phi^2}{2\mu_0 S} = \frac{\phi_m^2}{2\mu_0 S}\sin^2 \omega t = \frac{\phi_m^2}{4\mu_0 S}\left(1-\cos 2\omega t\right) \tag{8}$$

The magnitude of the Maxwell force varies with the flux density and the two are positively correlated. The frequency of Maxwell's force is twice the frequency of the industrial frequency, so the vibration noise is dominated by 100Hz.

II. B. 3) Effect of Lorentz force on reactor vibration noise

Reactor cores have air gaps, which generate leakage flux during normal operation. Energized windings in the leakage field will produce Lorentz force, causing periodic vibration of the winding. It is generally recognized that the insulating pads between the windings are elastic elements.

The reactor winding is subjected to a Lorentz force in the magnetic field of magnitude:

$$F_L = LIB \tag{9}$$

where, F_L is the magnitude of the Lorentz force; L is the length of the wire; I is the current.

It is known that the leakage field in the winding is proportional to the current, and at industrial frequency, the instantaneous current $i = I_m \cos \omega t$, I_m is the peak current. Therefore, the magnitude of the Lorentz force on the winding is:

$$F_L = ki^2 = \frac{1}{2} k I_m^2 \left(1+\cos 2\omega t\right) \tag{10}$$

where, k is the scale factor.

From Eq. (10), it can be concluded that the Lorentz force is a periodic function of frequency, which is twice the frequency of the working frequency, and the vibration noise of the windings is dominated by 100 Hz as the main frequency.

II. C. Optimization based on the forgotten least squares method

Enhanced self-immunity can effectively suppress mechanical resonance, and in the two-inertia system model, obtaining accurate inertia values and stiffness coefficients is also an important condition for realizing adaptive filtering. Therefore, the accurate identification of rotational inertia and other parameters is of great significance for the comprehensive optimization of electromagnetism and noise in core reactors.

II. C. 1) Forgetting the principle of least squares

The principle of the least squares method is shown in Figure 1. For a single-input, single-output continuous-time system, $u(k)$ is the input, $y(k)$ is the system observation output variable, and $e(k)$ is the system observation error.

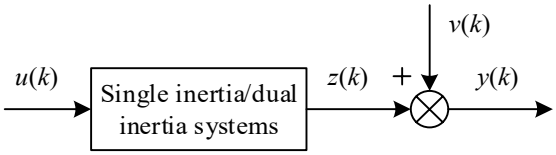

Figure 1: The principle of the least square method

According to Figure 1, the autoregressive model with control quantities is represented as follows:

$$y(k)=\frac{B(z)}{A(z)}u(k)+v(k) \tag{11}$$

where, z is the time shift operator, $u(k)$ and $y(k)$ are the input and output quantities in the discrete domain, $v(k)$ is the random noise term, and $A(z)$ and $B(z)$ are the discrete forms of the numerator-denominator of the transfer function in the inertial system, respectively.

The transfer function in the discrete domain of the system can be expressed in the following differential form:

$$\frac{B(z)}{A(z)}=\frac{b_0 z^{n_b}+b_1 z^{n_b-1}+\cdots+b_{n_b}}{z^{n_a}+a_1 z^{n_a-1}+\cdots+a_{n_a}} \tag{12}$$

where, n_a and n_b are the discrete orders of the denominator and numerator, respectively, and $a_i(i=1\sim n_a)$, $b_i(i=0\sim n_a)$ are the parameters to be recognized in the discrete domain of the least squares algorithm, respectively.

Equation (12) is transformed into the form of the k th output signal sample:

$$y(k)=-\sum_{i=1}^{n_a}a_i z(k-i)+\sum_{i=0}^{n_b}b_i z(k-i) \tag{13}$$

Transform the above equation into least squares format as:

$$y(k)=\varphi^T(k)\theta \tag{14}$$

where the autoregressive vector $\varphi^T(k)$ and the parameter vector θ are respectively:

$$\begin{cases}\varphi(k)=[-y(k-1),\cdots,-y(k-n_a),u(k-1),\cdots,u(k-n_b)]\\ \theta=[a_1,\cdots,a_{n_a},b_0,\cdots,b_{n_b}]\end{cases} \tag{15}$$

The difference between the actual output and the estimated output is:

$$v(k)=y(k)-\hat{y}(k) \tag{16}$$

The square of the sum of the errors of N times all observations, defined as the evaluation function of the RLS algorithm, can be expressed as follows:

$$J = \sum_{k=1}^{N} v^2(k) = \sum_{k=1}^{N} \left[y(k) - \hat{y}(k) \right]^2 \tag{17}$$

The least squares estimate of the parameters corresponds to the parameter $\hat{\theta}$ for which the objective function J takes on a very small value, so the derivative of $\hat{\theta}$ is found for the objective function and takes on the value of zero, i.e.:

$$\frac{\partial J}{\partial \hat{\theta}} = 2\phi^T \phi \hat{\theta} - 2\phi^T Y = 0 \tag{18}$$

If $\phi^T \phi$ is a positive definite matrix, Eq. (18) has a solution and is expressed as:

$$\hat{\theta} = (\phi^T \phi)^{-1} \phi^T Y \tag{19}$$

where, Y and ϕ are the output matrix of N observations and the historical input-output vector matrix.

In this control system application, the input signal i_q sampled by the least squares method and the rotational speed output signal ω_m are smooth random signals, so $\phi^{\mathrm{T}} \phi$ is a positive definite matrix. In addition, if the objective function is made to take a very small value, it should also satisfy that its second order derivative is greater than zero. That is, $\frac{\partial^2 J}{\partial \hat{\theta}^2} = 2\phi^T \phi > 0$, in this case the obtained $\hat{\theta}$ is the optimal identification parameter of the least squares method.

From equation (19), it can be seen that the least squares method needs to calculate the inverse of the data matrix every time the data are processed, which is computationally cumbersome, and in order to be used in the online estimation of the parameters, it needs to be reduced to a recursive form. Combining the matrix inverse lemma and Eq. (19), the covariance matrix $P(k)$ and the gain vector $X(k)$ are introduced, and the iterative form of the recursive least squares method can be found as:

$$\begin{cases} \hat{\theta}(k) = \hat{\theta}(k-1) + K(k)[y(k) - \varphi^T \hat{\theta}(k-1)] \\ K(k) = \dfrac{P(k-1)\varphi(k)}{1 + \varphi^T(k) P(k-1) \varphi(k)} \\ P(k) = [I - K(k)\varphi^T(k)] P(k-1) \end{cases} \tag{20}$$

For the recursive least squares method, with the increase of data collection samples, the proportion of the newly collected sample data in the global data will be reduced, and the accumulation of data will appear the phenomenon of “data saturation”. In order to reduce the impact of old data on the identification results, and increase the proportion of new data in the identification analysis, we can add the forgetting factor λ in the recursive least squares method. Certain corrections are made to the performance weights. Then equation (20) can be rewritten as:

$$J = \sum_{k=1}^{N} \lambda^{N-k} \left[y(k) - \varphi^T \hat{\theta} \right]^2 \tag{21}$$

Then the recursive least squares iteration with forgetting factor takes the form:

$$\begin{cases} \hat{\theta}(k) = \hat{\theta}(k-1) + K(k)[y(k) - \varphi^T \hat{\theta}(k-1)] \\ K(k) = \dfrac{P(k-1)\varphi(k)}{\lambda + \varphi^T(k) P(k-1) \varphi(k)} \\ P(k) = \lambda^{-1}[I - K(k)\varphi^T(k)] P(k-1) \end{cases} \tag{22}$$

where the forgetting factor λ is usually taken in the range of $0.9 \le \lambda \le 1$, it can be seen that Eq. (22) degenerates to the regular recursive least squares formula when λ is taken as 1. By appropriately choosing the initial value $P(0)$ and $\hat{\theta}(0)$, combined with the original collected data of the system, then the identification results in the discrete domain can be obtained. By transforming the discrete domain to the frequency domain, the final parameter identification results can be obtained.

II. C. 2) Identification of mechanical parameters

For the two-inertia system, more mechanical parameters need to be recognized compared with the single-inertia system because the flexible characteristics of the drive shaft cannot be neglected. Under no-load conditions, the two-inertia system transfer function is expressed as shown in Eq. (23), and the motor angular velocity transfer function can be written as:

$$\omega_m(s)=\frac{J_1s^2+B_ss+K_s}{J_mJ_1s^3+(J_m+J_1)B_ss^2+(J_m+J_1)K_ss}T_e -\frac{B_ss+K_s}{J_mJ_1s^3+(J_m+J_1)B_ss^2+(J_m+J_1)K_ss}T_l \tag{23}$$

Then the identification model in the frequency domain of the two-inertia system can be expressed as:

$$\omega_m(s)=\frac{B(s)}{A(s)}i_q-\frac{C(s)}{A(s)}T_l \tag{24}$$

where, $\begin{cases}A(s)=J_mJ_1s^3+(J_m+J_1)B_ss^2+(J_m+J_1)K_ss\\B(s)=K_t(J_1s^2+B_ss+K_s)\\C(s)=B_ss+K_s\end{cases}$.

To apply the forgotten least squares method, it is necessary to convert the frequency domain transfer function to the discrete domain by rewriting Eq. (24) under the discrete domain as:

$$\omega_m(z)=\frac{\theta_1z^2+\theta_2z+\theta_3}{z^3+\theta_6z^2+\theta_7z}i_q(z)+\frac{\theta_4z+\theta_5}{z^3+\theta_6z^2+\theta_7z}T_l(z) \tag{25}$$

Writing the above equation in least squares form, the corresponding discriminant data vector $\varphi(k)$ and parameter vector θ are:

$$\begin{cases}\varphi(k)=[i_q(k-1),i_q(k-2),i_q(k-3),T_l(k-2)\\T_l(k-3),-\omega_m(k-1),-\omega_m(k-2)]\\\theta=[\theta_1,\theta_2,\theta_3,\theta_4,\theta_5,\theta_6,\theta_7]^T\end{cases} \tag{26}$$

From the above equation, the data vector consists of three observations i_q, T_l, ω_m sampled instantaneous values, and corresponds to the parameters of the seven parameter vectors, by choosing the appropriate initial values of the vectors, $P(0)$ and $\hat{\theta}(0)$, and combining with the systematic sampling data, the values of the parameter vectors can be calculated by the forgotten least squares iteration formula. The values of the parameter vectors can be calculated by the forgotten least squares iteration formula. It is worth noting that the parameters θ_4 and θ_5 generated by the loaded part of the action are added to θ after loading. These two parameters are involved in the iterative process only in the form of operations, but not in the transformation process from the discrete domain to the frequency domain, and the identification process is completed by the first model of Eq. (25). The values of the parameter vectors θ_1, θ_2, θ_3, θ_6, θ_7 in the discrete domain are computed from the iteration, and by transforming them to the frequency domain, the values of J_m, J_l, B_s, and K_s can be recognized.

III. Simulation experiments of vibration damping effect of core reactor under optimized scheme

III. A. Vibration characterization of core reactors

The root causes of reactor vibration lie in the Maxwell force between the core cakes and the magnetostrictive force of the electrical material samples. In order to better investigate the roles of the two forces in the reactor vibration, this paper quantitatively analyzes the reactor vibration under Maxwell force and magnetostrictive force according to the magnetic-mechanical coupling model of the reactor established earlier, and further investigates the effects of external stresses on the reactor vibration.

The vibration and stress distribution of the reactor at any moment such as t=0.015s are selected for analysis. For a structural body, its magnetic field and vibration distribution is a general case of spatial distribution that does not

change with the excitation, but the field value is a function that changes with time as the excitation source changes. In order to study the vibration characteristics of the reactor more clearly and to visualize the vibration distribution, this paper calculates the curves of the vibration displacements with time for the experimental test points under the action of Maxwell's force and magnetostrictive force respectively, and the results of their action are shown in Fig. 2 (a~b) respectively.

The electromagnetic force and magnetostrictive force have different effects in the x, y and z directions, and the phase difference between the two in the x and z directions is 180 degrees, which cuts down the effect of each other. At the same time can also be found that the vibration is mainly x, z component, y component is approximately zero, indicating that the electromagnetic force and magnetostrictive force generated by the vibration effect of the core of the up and down vibration and vibration deformation to the two sides of the yoke, in the y direction caused by vibration displacements are small, negligible. In addition, it can be seen, no matter what kind of force, vibration in the z-direction component is greater than the x, y-direction component. Therefore, external fastening devices and other measures can be taken to increase the vertical force on the reactor core to reduce the vibration amplitude of the reactor in the vertical direction.

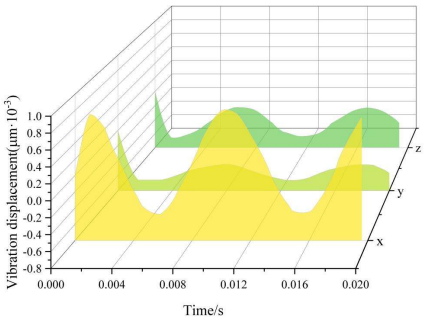

(a)Maxwell Force

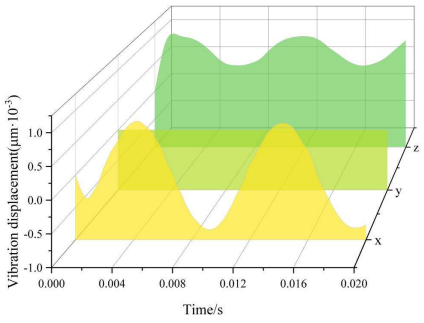

(b)Magnetostrictive force

Figure 2: Distribution of vibration displacement of the reactor under different stresses

In addition to displacement and stress, vibration acceleration is also one of the characteristic physical quantities that characterize the magnitude of vibration of an object. In this paper, taking the experimental test point as the observation point, the vibration acceleration of the reactor in the x, y and z directions is shown in Fig. 3 under the consideration of Maxwell's force and magnetostrictive force together. From Fig. 3, it can be found that the vibration acceleration of the reactor in the z-axis is maximum, which is about 1.8287 m/s², and the vibration is approximately sinusoidal waveform. Compared with the z-direction, the vibration acceleration in the x,y-direction are different degrees of distortion, which is because the magnetic inductance in the junction of ferromagnetic material and air occurs outward curvature, the edge of the magnetic field distribution is uneven, resulting in the generation of high harmonics in the system.

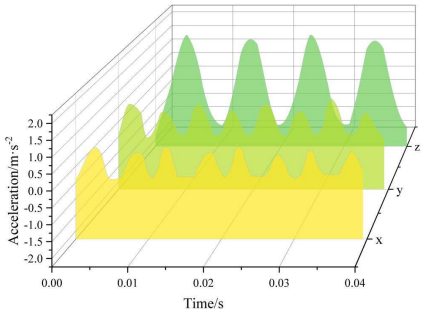

Figure 3: Vibration acceleration under the combined effect

III. B. Simulation calculation of electromagnetic-mechanical coupling of iron core

Four measurement points are selected on the core, which are located inside the core column, at the magnetic split on the core, at the corner of the upper yoke and the side yoke, and at the center of the side yoke. The winding force

is divided into axial and spoke direction two positions, axial electromagnetic force mainly acts in the winding ends, while the spoke electromagnetic force acts in the winding as a whole, so respectively in the center of the winding and the top position to choose two displacement measurement points.

The frequency domain analysis of the core displacement results, the displacement frequency domain results are shown in Figure 4. Through the core displacement frequency domain analysis, it can be clearly seen that the reactor core vibration frequency of the main frequency of 100Hz, and 50Hz even times the frequency content are greater than other frequencies, the core vibration displacement frequency and reactor vibration noise frequency components close to.

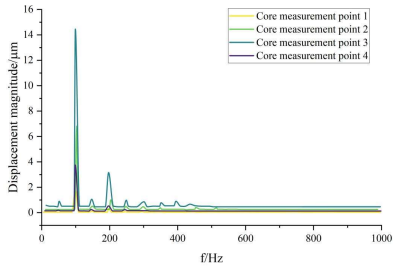

Figure 4: Spectrum of vibration measurement points for the core

The same frequency domain analysis of the winding measurement points, to obtain its displacement spectrum shown in Figure 5. Through the core and winding frequency domain analysis, it can be found that the vibration frequency of the reactor and noise measured spectrum of the main frequency are 100Hz, and 50Hz octave content are greater than other frequencies. This proves the correctness of the electromagnetic-mechanical coupling calculation system model of the core reactor built in this paper.

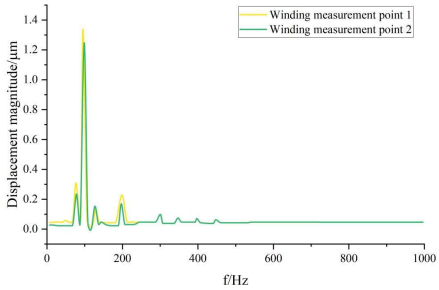

Figure 5: Spectrum of winding vibration measurement points

III. C. Analysis of the effect of the optimization scheme

In order to verify the validity of this paper's comprehensive electromagnetic and noise optimization scheme based on the least squares method, three mainstream optimization schemes are introduced for comparison experiments. The statistical energy model of the reactor acoustic package corresponding to the original scheme and the four optimization schemes is established, and the noise of the evaluation measurement point at 1m in the center directly in front of the reactor cabinet is predicted, and its 1/3-octave curve is shown in Fig. 6. Comparing this paper's scheme with the original scheme, it can be seen that the sound insulation of this paper's scheme can be up to 14.6dB(A), and its sound insulation for high-frequency noise is larger than that for low-frequency noise, so the sound insulation performance is better, and it meets the design requirements. Compared with the three comparative schemes, the overall sound insulation performance of the reactor acoustic package in this paper is the best [23]-[25] .

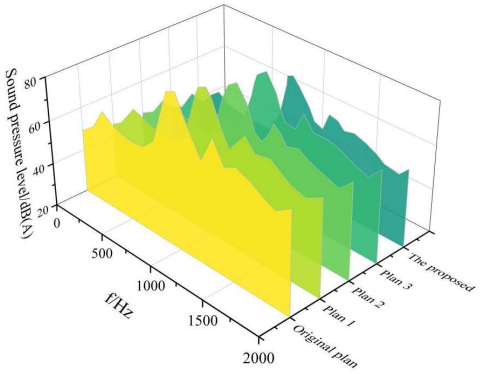

Figure 6: 1/3 octave band curves under different optimization schemes

The scheme of this paper is used to modify the reactor acoustic package and prototype validation test. The 1/3-octave difference curves of each measurement point of the reactor acoustic package before and after optimization are shown in Figure 7. After optimization, the 1/3-octave curves of measurement points B and C at 1m outside the reactor cabinet are basically the same, and the total sound pressure level is reduced by 10.2dB(A) and 11.5dB(A) respectively compared with that before optimization. Taking into account the differences in the background noise of the two tests, the comprehensive noise reduction effect is more than 10.9dB(A). Before and after the optimization, the noise SPL sizes at the A measurement point inside the reactor cabinet are almost equal, which further verifies the consistency of the two test sources and the accuracy of the assessment of the noise reduction effect. After adopting the optimization scheme in this paper, the temperature rise of the reactor does not increase significantly, indicating that the optimization scheme can meet the requirements of engineering applications.

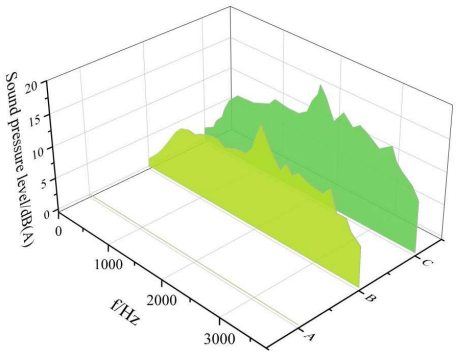

Figure 7: 1/3 octave difference curves for each measurement point

IV. Conclusion

In this paper, the electromagnetic and noise optimization scheme of Fe-based soft magnetic composite core reactor based on the least squares method is designed, and the vibration damping effect of the core reactor under the optimization scheme is explored through simulation experiments.

The electromagnetic force and magnetostrictive force have different effects in the x, y and z directions, and the phase difference between the two in the x and z directions is 180 degrees, which reduces the effect of each other. Vibration is mainly x, z component, y component is approximately zero, no matter what kind of force action, vibration in the z direction is greater than the component in the x, y direction. Under the consideration of Maxwell's force and magnetostrictive force together, the vibration acceleration of the reactor in the z-axis is the largest, which is about 1.8287m/s², and the vibration is approximately sinusoidal waveform. Compared with the z-direction, the vibration acceleration in the x- and y-directions are distorted to different degrees. Through the core and winding frequency domain analysis, it can be found that the reactor vibration frequency and noise measured spectrum main frequency are 100Hz, and 50Hz octave content are greater than other frequencies. This proves the correctness of the electromagnetic-mechanical coupling calculation system model of the core reactor built in this paper.

Comparing this paper's scheme with the original scheme, it can be seen that the sound insulation of this paper's scheme can be up to 14.6dB(A), and its sound insulation for high-frequency noise is larger than that for low-frequency noise, so the sound insulation performance is better and meets the design requirements. Compared with the three comparative schemes, the overall acoustic performance of the reactor acoustic package in this paper is

the best. The 1/3-octave curves of measurement points B and C at 1m outside the reactor cabinet are basically the same after the optimization of this paper, and the total sound pressure level is reduced by 10.2dB(A) and 11.5dB(A) respectively compared with that before optimization, and the comprehensive noise reduction effect reaches more than 10.9dB(A), and the size of the noise level of the measurement point A inside the reactor cabinet before and after the optimization is almost the same. Comparison experiments prove the effectiveness of the optimization scheme in this paper, which can meet the requirements of engineering applications.

Funding

This work was supported by State Grid Hebei Electric Power Co., LTD. Science and Technology Project funding: A new type of low noise core reactor based on Fe based soft magnetic composite material is developed (5204CZ240002).

References

[1] Wong, H. G., Speight, V. L., & Filion, Y. R. (2017). Impact of urban development on energy use in a distribution system. Journal - American Water Works Association, 109(1), E10-E18.

[2] Velásquez, R. M. A., & Lara, J. V. M. (2019). Methodology for failure analysis in shunt reactor by electromagnetic influence caused by high vibration in overload condition. Engineering failure analysis, 104, 589-608.

[3] Zhu, L., Wang, Q., Sha, R., & Koh, C. S. (2021). A New Structure of a Gap-Reactor to Reduce Electromagnetic Vibrations. Journal of Electrical Engineering & Technology, 16, 1437-1443.

[4] Ma, Y., Song, W., Gao, J., Liu, Y., Shang, Y., Zhao, W., & Yang, F. (2025). Integrated electromagnetic and noise optimization design of Fe-based soft magnetic composite core reactor based on genetic algorithm. J. COMBIN. MATH. COMBIN. COMPUT, 127, 5125-5148.

[5] Huang, H., Zhang, R., Sun, H., Zhang, J., & Wang, J. (2023). High density Fe-based soft magnetic composites with nice magnetic properties prepared by warm compaction. Journal of Alloys and Compounds, 947, 169460.

[6] Wang, J. (2013). Design method of flow distribution in nuclear reactor systems. Chemical Engineering Research and Design, 91(4), 595-602.

[7] Khan, M. S., Bai, Y., Huang, Q., Xu, C., Sun, L., Zou, X., & Wang, L. (2020). Conceptual design and optimization of power generation system for lead-based reactor. Applied Thermal Engineering, 168, 114714.

[8] Sun, H., Ma, P., Liu, X., Tian, W., Qiu, S., & Su, G. (2018). Conceptual design and analysis of a multipurpose micro nuclear reactor power source. Annals of Nuclear Energy, 121, 118-127.

[9] Du, X., Tao, Y., Zheng, Y., Wang, C., Wang, Y., Qiu, S., ... & Zhai, Z. A. (2021). Reactor core design of UPR-s: a nuclear reactor for silence thermoelectric system NUSTER. Nuclear Engineering and Design, 383, 111404.

[10] Komarzyniec, G., & Aftyka, M. (2023). Analysis of plasma reactor interaction with the power grid depending on the power supply design. Applied Sciences, 13(4), 2279.

[11] Huang, H., Tang, Y., Ren, L., Shi, J., Li, J., Xu, Y., ... & Wang, Z. (2021). Simplified design of R-SFCL with shunt reactor for protecting HTS cable in distribution network. IEEE Transactions on Applied Superconductivity, 31(8), 1-5.

[12] Meng, B., Hou, J., Ning, F., Yang, B., Zhou, B., & Yu, R. (2019). Low-loss and high-induction Fe-based soft magnetic composites coated with magnetic insulating layers. Journal of Magnetism and Magnetic Materials, 492, 165651.

[13] Peng, Y., Yi, Y., Li, L., Ai, H., Wang, X., & Chen, L. (2017). Fe-based soft magnetic composites coated with NiZn ferrite prepared by a co-precipitation method. Journal of Magnetism and Magnetic Materials, 428, 148-153.

[14] Birčáková, Z., Kollár, P., Füzer, J., Bureš, R., & Fáberová, M. (2020). Magnetic properties of selected Fe-based soft magnetic composites interpreted in terms of Jiles-Atherton model parameters. Journal of Magnetism and Magnetic Materials, 502, 166514.

[15] Liu, J., Peng, X., Li, J., Yang, Y., Xu, J., Hong, B., ... & Wang, X. (2021). Highly improved middle to higher frequency magnetic performance of Fe-based soft magnetic composites with insulating Co2Z hexaferrites. Journal of Magnetism and Magnetic Materials, 538, 168297.

[16] Sun, H., Zhou, G., Guo, Z., Wang, C., Wang, J., & Zong, C. (2022). Efficient synthesis of TiO2-coated layer for Fe-based soft magnetic composites and their regulation mechanism analysis on magnetic properties. Journal of Materials Science: Materials in Electronics, 33(17), 13956-13967.

[17] Neamţu, B. V., Pszola, M., Vermeşan, H., Stoian, G., Grigoraş, M., Opriş, A., ... & Chicinaş, I. (2021). Preparation and characterisation of Fe/Fe3O4 fibres based soft magnetic composites. Ceramics International, 47(1), 581-589

[18] Zhang, Z., Zhang, Z. D., Cai, Y. F., Zhang, Y., Wu, Y., Zhu, H. H., ... & Wang, W. H. (2024). A unique Fe-based soft magnetic alloy and its magnetic softening mechanism. Journal of Alloys and Compounds, 1002, 175161.

[19] Remus, N., Toulabi, M. S., Mukundan, S., Dhulipati, H., Li, W., Novak, C., & Kar, N. C. (2020, August). Electromagnetic noise and vibration in pmsm and their sources: An overview. In 2020 IEEE Canadian Conference on Electrical and Computer Engineering (CCECE) (pp. 1-4). IEEE.

[20] Lin, F., Zuo, S., & Wu, X. (2016). Electromagnetic vibration and noise analysis of permanent magnet synchronous motor with different slot - pole combinations. IET Electric Power Applications, 10(9), 900-908

[21] Guo, J., Geng, J., Lü, F., & Pan, Y. (2021). Optimisation design of double-column multi-gap reactor core structure for noise reduction. International Journal of Electrical Power & Energy Systems, 133, 107165.

[22] Yuan, F., Yuan, Z., Chen, L., Wang, Y., Liu, J., He, J., & Pan, Y. (2017). Thermal and electromagnetic combined optimization design of dry type air core reactor. Energies, 10(12), 1989.

[23] H. Wang, J. Wang, L.C. Li, et al. Misalignment tolerance improvement of loosely coupled transformer with ferromagnetic materials via genetic algorithm, Electrical Materials and Applications, 1 (2) e70003, 2024.

[24] Y.T. Wang, X. Li, Z.T. Gao, et al. Analysis and calculation of no-load leakage flux coefficient for arc motors, Electrical Materials and Applications, 2 (1) e70013, 2025.

[25] C.Y. Liu, F.Y. Yang, Y. Han, et al. Advances in high magnetic induction and low loss Fe-based nanocrystalline alloys, Electrical Materials and Applications, 2 (2) e70012, 2025.